Deciphering population-level response under spatial drug heterogeneity on microhabitat structures

Zhijian Hu[1,2,3*], Kevin Wood[1,3,4]

1 Department of Biophysics, University of Michigan, Ann Arbor, USA
2 Department of Mathematics, University of Michigan, Ann Arbor, USA
3 Center for the Study of Complex Systems, University of Michigan, Ann Arbor, USA
4 Department of Physics, University of Michigan, Ann Arbor, USA

* zhijianh@umich.edu

Abstract

Bacteria and cancer cells live in a spatially heterogeneous environment, where migration shapes the microhabitat structures critical for colonization and metastasis. The interplay between growth, migration, and microhabitat structure complicates the prediction of population responses to drugs, such as clearance or sustained growth, posing a longstanding challenge. Here, we disentangle growth-migration dynamics and identify that population decline is determined by two decoupled terms: a spatial growth variation term and a microhabitat structure term. Notably, the microhabitat structure term can be interpreted as a dynamic-related centrality measure. For fixed spatial drug arrangements, we show that interpreting these centralities reveals how different network structures, even with identical edge densities, microhabitat numbers, and spatial heterogeneity, can lead to distinct population-level responses. Increasing edge density shifts the population response from growth to clearance, supporting an inversed centrality-connectivity relationship, and mirroring the effects of higher migration rates. Furthermore, we derive a sufficient condition for robust population decline across various spatial growth rate arrangements, regardless of spatial-temporal fluctuations induced by drugs. Additionally, we demonstrate that varying the maximum growth-to-death ratio, determined by drug-bacteria interactions, can lead to distinct population decline profiles and a minimal decline phase emerges. These findings address key challenges in predicting population-level responses and provide insights into divergent clinical outcomes under identical drug dosages. This work may offer a new method of interpreting treatment dynamics and potential approaches for optimizing spatially explicit drug dosing strategies.

Introduction

Healthcare-related cell communities, such as bacterial infections and cancer, have increasingly been recognized as complex ecosystems over the past decades [1–3]. These systems exhibit emergent collective behaviors, including antibiotic resistance and cancer invasion, which arise from the interplay of ecological and evolutionary processes. The complex interactions between different phenotypes and genotypes have inspired novel therapeutic approaches, such as containment strategies and adaptive therapies [4–8], which leverage competition between cell types. From a dynamical systems perspective, drugs constitute an integral part of the environment, and their interactions with

cells—particularly under spatially heterogeneous drug distributions—have gained attention in recent years [5, 9–39].

At the evolutionary timescale, studies on cancer have demonstrated that spatial drug heterogeneity can accelerate the evolution of drug resistance [10], shortening the time between initial treatment and the emergence of resistant clones at detectable levels. This phenomenon has been captured in minimal two-well models and extended ladder models, where differences in drug concentration modulate growth rates [16, 17]. Similar acceleration effects have been observed in bacterial populations through laboratory experiments [11, 12], though recent theoretical work using mean first passage time models suggests that spatial heterogeneity can either accelerate or decelerate resistance evolution depending on mutation and migration rates [10, 36, 39, 40]. These contrasting outcomes underscore the complexity of resistance evolution and suggest that optimal spatial drug heterogeneity design could help slow resistance development.

At the ecological timescale, similar variability is observed in patient outcomes. Even under identical drug dosages, patients exhibit different levels of pathogen or cancer cell clearance between the first treatment and the final day of therapy. For instance, despite a standard 14-day antibiotic treatment regimen, approximately 20% of patients fail to achieve sufficient clearance of H. pylori [41]. Similarly, cancer patients face recurrence risks due to insufficient clearance [5, 42, 43], which may be influenced by spatial heterogeneities in drug absorption and pharmacokinetics/pharmacodynamics (PK/PD) [25]. Unlike well-mixed laboratory conditions, the in vivo tumor and microbial environments exhibit spatial complexity, making traditional well-mixed drug-dose response measurements insufficient for predicting clinical outcomes. Recent work [44] has modeled population-level responses as an eigenvalue problem, where cell survival or extinction is governed by the interplay of spatial growth, migration, and microhabitat connectivity in a one-dimensional setting. This framework has been extended to model the emergence of multidrug resistance under natural selection [45]. However, the entanglement of structural, migratory, and growth-related factors in these eigenvalue formulations limits their interpretability. Additionally, clinical applications require extending these results beyond one-dimensional models to account for multiple discrete microhabitat scenarios such as cancer metastasis [46–50], lymph node networks [51–53], and bacterial translocation across body compartments [15, 54, 55].

To better understand how spatial drug heterogeneity shapes population-level responses—specifically, whether cell populations grow or decline—we develop a minimal growth-migration model on a microhabitat network. This model incorporates growth rates constrained by drug-dependent maximum and minimum values. We theoretically decouple structural effects from spatial growth variations induced by drug heterogeneity by introducing a novel dynamic-related centrality measure. This reformulation transforms the problem from a dynamical analysis into a network-theoretic framework. Given a predefined microhabitat structure, migration rate, and maximum death rate (or equivalently, minimum growth rate, which depends on drug-cell interactions), we show that population survival or decline is determined solely by the spatial growth rate relative to the maximum death rate. This provides an efficient criterion for evaluating population clearance. Interestingly, we find that increasing microhabitat connectivity mimics the effect of increasing migration rates, leading to a gradual transition from population growth to decline. Moreover, for a fixed microhabitat structure, population dynamics are controlled by the spatially averaged growth rate and migration rate, with diverging outcomes depending on spatial drug distribution. We identify a sufficient condition for robust population decline that remains valid regardless of the spatial arrangement of drugs. Notably, this condition becomes exact when all microhabitats form a fully connected network (i.e., a complete graph). Different environment-cell pairs exhibit varying ranges of drug-induced growth rates, leading to different maximum

growth-to-death ratios. We finally explore how these variations influence the stability of population decline, and identify a threshold beyond which the decline phase remains unchanged, regardless of the specific growth-to-death ratio. This result has been compared with experimental bacterial data to interpret the critical ratio and provide clinical insights into population decline

Health-related complex systems, such as cancer and bacterial infections, require deeper exploration to disentangle the contributions of various factors to treatment outcomes. Our theoretical framework provides a generalizable method for assessing population decline under spatial drug heterogeneity. This model could serve as a foundation for more complex extensions, incorporating additional environmental and interspecies interactions. Clinically, our findings may inform the design of spatially explicit dosing strategies for more effective infection and cancer treatment.

Basic set-up of model system

Cell populations like bacteria, or cancer cells, can actively or passively move between different sites by migration or metastasis. When accounting for fluctuations in population growth and the stochastic nature of drug-induced clearance [56], the system can be described using stochastic microscopic dynamics governed by a master equation (see SI). However, in human bodies, where bacterial and cancer cell populations typically exceed thousands, we can apply the Van Kampen approximation [57]. This allows us to ignore microscopic dynamic details and derive a simplified macroscopic growth-migration equation

$$\frac{du}{dt} = -\beta L u + G u = \Omega u \tag{1}$$

This is equivalent to a linearized exponential growth from logistic growth, by ignoring the competition or density-dependent effect, where

$$G = \begin{pmatrix} g_1 & & & \\ & g_2 & & \\ & & \ddots & \\ & & & g_N \end{pmatrix}$$

is a diagonal matrix describing growth rates induced by drug at different microhabitats. And L is the Laplacian matrix describing the multi-microhabitat structure. β describes the migration rate and $u = (u_1, u_2, \cdots, u_N)^T$ describes the population densities on different microhabitats. N is the total number of microhabitats. Since drug-induced growth rates $\{g_i\}$ cannot be infinite, we require $g_i \in [d_0, g_0]$, where $d_0 < 0$ is the maximum death rate, and $g_0 > 0$ is the maximum growth rate or drug-free growth rate, depending on drug type and cell type, or other environmental factors like nutrition [58–60]. For example, single bactericidal drug like Ampicillin can be fitted into a hill fuction to get maximum growth rate at a drug-free environment, or the maximum death rate when the AMP concentration is extremely high [61].

Since the drug concentration must be sufficiently high to eliminate cancer or bacterial cells, we require that the spatially averaged growth rate satisfies $\langle g \rangle = \frac{\sum_i^N g_i}{N} < 0$. For population decline or clearance, the condition $\Omega = G - \beta L \prec 0$ must hold, or equivalently, the largest eigenvalue $\lambda_0 = \|\Omega\| = \|G - \beta L\| < 0$. However, solving this exactly is typically intractable. Applying first-order perturbation theory, as in recent studies [44, 45], we approximate the largest eigenvalue as

$$\lambda_0 \approx \langle g \rangle + \langle u_0 | \, \delta g \, | u_0 \rangle = \langle g \rangle$$

Since $u_0 = \frac{1}{\sqrt{N}}(1, 1, \ldots, 1)^T$, we obtain $\langle u_0 | \, \delta g \, | u_0 \rangle = 0$, indicating that this approximation only captures well-mixed effects while neglecting spatial drug distribution and multi-microhabitat structure. Higher-order approximations may be necessary but are challenging to compute. Instead of relying on perturbation theory, we derive an exact solution for the clearance or decline criterion. Decomposing G as $G = -|d_0| \, I + U_\delta U_\delta^T$, where I is the identity matrix and U_δ is an orthogonal diagonal matrix (see SI for details), we show that the condition $\Omega = G - \beta L \prec 0$ is equivalent to

$$\max C_i \delta_i < 1 \tag{2}$$

where $C_i = \sum_{k=1}^{N} \frac{V_{ik}\left(V^{-1}\right)_{ki}}{1+\frac{\beta}{|d_0|}\omega_k}$ is a dynamic-related centrality, with V and ω_k representing the eigenvector matrix and eigenvalues of the Laplacian matrix L, respectively. Additionally, $\delta_i = \frac{g_i - d_0}{|d_0|}$ quantifies the relative growth deviation at microhabitat i compared to the maximum drug-induced death rate. For a fixed $\langle g \rangle, C_i\left(\frac{\beta}{|\langle g \rangle|}; \{v_i\}, \left\{v_i^{(-1)}\right\}, \{\omega_k\}\right)$ encodes migration and microhabitat structure information, while δ_i captures only the spatial growth profile. Thus, our criterion effectively decouples the contributions of spatial growth and microhabitat structure. In a spatially homogeneous drug environment, this criterion simplifies to $C_{\max} < \frac{1}{\delta}$, where δ is the relative growth deviation across all microhabitats. This result mirrors the epidemic outbreak condition in susceptible-infectious-susceptible (SIS) network dynamics [62–65], where $C_{\max}$ corresponds to the largest eigenvalue of the adjacency matrix and δ represents the effective infection rate.

In this study, since the population decline criterion involves two key terms, C_i and δ_i, we structure our findings as follows: a) Given a predefined spatial drug heterogeneity $\{\delta_i\}$ or $\{g_i\}$, we analyze how different microhabitat structures C_i influence population-level responses. b) Given a known multi-microhabitat structure C_i, we explore the effects of varying $\{g_i\}$ on population decline.

Microhabitat structure effects under a given spatial drug heterogeneity

Without loss of generality, here we set $\langle g \rangle = -1$ and fix $\beta = 1$. We aim to investigate the impact of microhabitat structures on spatial drug responses. Specifically, we focus on: a) How different microhabitat structures with the same connectivity influence population responses. b) How varying connectivity levels shape spatial drug responses across different microhabitat structures, and how this can be predicted by the dynamic-related centrality C.

Distinct population responses induced by different multi-microhabitat structures

Starting from a fixed spatial drug heterogeneity (see Figure 1A), we first demonstrate how different multi-microhabitat structures lead to distinct population responses, which can be precisely captured by $(C\delta)_{\max}$. The dynamic-related centralities C are visualized for two different multi-microhabitat structures, with color gradients indicating different values (see Figure 1B). All values of C are upper bounded by 1 (see SI). Different transparencies represent varying growth rate values.

Notably, the locations of $g_{\max}$ (or $\delta_{\max}$), $C_{\max}$, and $(C\delta)_{\max}$ do not necessarily coincide. We can approximate $C\delta$ directly from the visualized networks by observing the color and transparency of microhabitats(nodes), which are highlighted in different colors. The adjacent bar plots reveal that in one structure, at least one $C\delta$ value

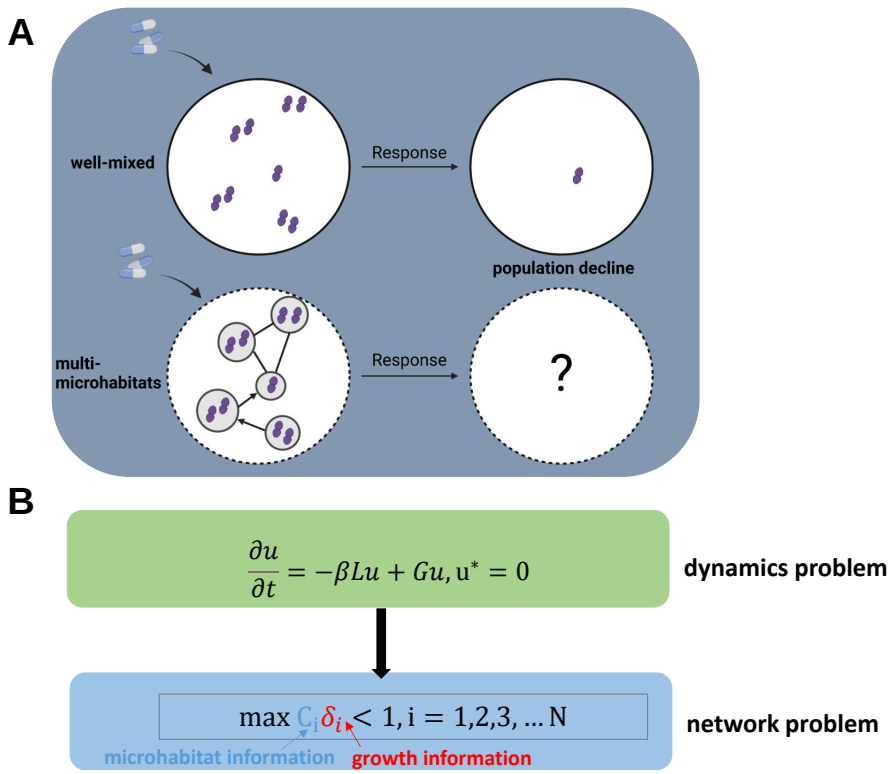

Figure 1. Illustration of Population Response Under Drug Exposure and Theoretical Condition for Population Decline. A. Example of multiple bacterial microhabitats and their diverging population responses. Despite receiving the same drug dose, bacterial populations may exhibit microhabitat-dependent responses, even when the population would decline in a well-mixed environment. **B.** Theoretical condition for population decline, formulated by transforming the dynamical problem into a network problem. This framework effectively decouples microhabitat structure from spatial growth dynamics, providing a clearer criterion for predicting population decline.

exceeds 1, whereas in the other, all values remain below 1. Consequently, the first multi-microhabitat structure leads to population growth, while the second results in decline, as illustrated by the spatial-temporal dynamics in Figure 1C. Our exact theoretical criterion thus serves as a powerful predictive tool for population responses without requiring detailed dynamic simulations. Interestingly, this newly defined centrality is inversely proportional to node degree, contrasting with many conventional centrality measures (see SI). It bears similarity to betweenness centrality, suggesting that in a given multi-microhabitat structure, the most effective drug targeting should focus on sparsely connected habitats to maximize bacterial clearance.

Increased connectivity accelerates centrality-predicted population decline

Since dynamic-related centrality reflects the importance of edge number, it also suggests that increasing the average number of edges or connection density may enhance the likelihood of $\max C\delta < 1$, thereby increasing the probability of population decline. To

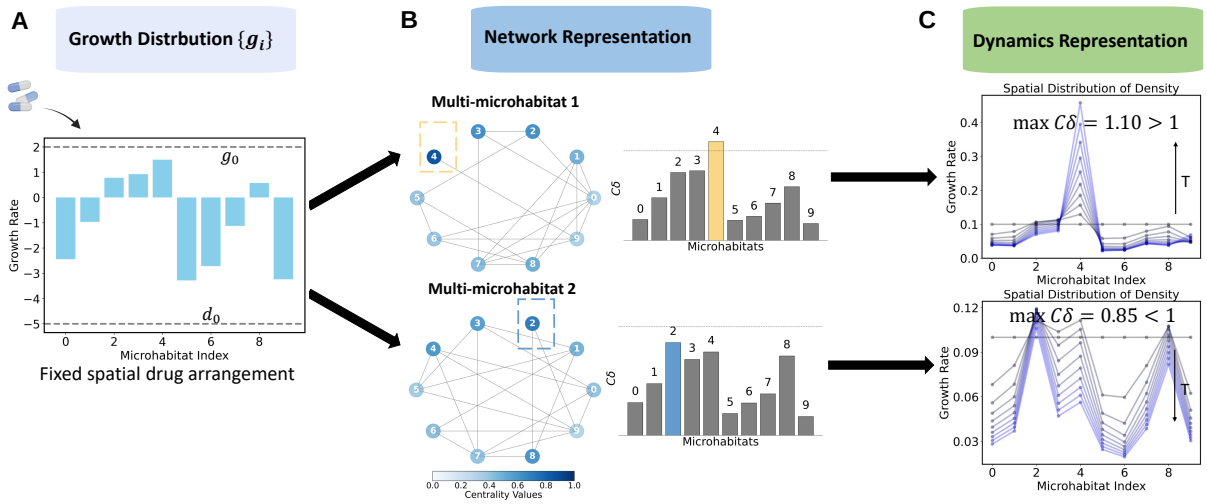

Figure 2. Different microhabitat structures with the same spatial growth distributions induce different population responses, explained by our exact criterion. A. Example distribution of spatial growth rates across 10 connected microhabitats. Growth rates are bounded by the drug-related maximum growth rate and death rate, represented by grey dashed lines. **B.** Two different microhabitat structures with the same number of microhabitats and migration connections, along with their corresponding $C\delta$ values shown as bar plots. In each structure, colors indicate dynamic-related centrality values C, while different transparencies represent relative growth δ. The microhabitat with the highest $C\delta$ in each structure is highlighted with a triangle, colored light yellow for population growth and light blue for population decline, as confirmed by the adjacent bar plots. Notably, the microhabitat with the highest dynamic-related centrality C does not necessarily correspond to the highest $C\delta$. **C.** Two spatial dynamic configurations demonstrating different population responses. The grey dashed line represents the initial population density. The dynamics induced by microhabitat 1 exhibit a growth trend, consistent with our theoretical prediction, while those induced by microhabitat 2 show a decline trend.

investigate this, we tune the edge density $\rho = \frac{|E|}{\binom{N}{2}}$, defined as the ratio of the total number of edges in a given graph to the number of edges in a complete graph, and examine its effect on $\max C\delta$.

Using 1000 stochastic samples from random graph for each edge density, we observe that as edge density increases, $\max C\delta$ decreases rapidly and eventually crosses the critical threshold $\max C\delta = 1$ (see Figure 2). Figure 2A illustrates four different multi-microhabitat structures with increasing edge densities, where the colors gradually fade to white, indicating decreasing $C\delta$ values. This finding suggests that densely connected microhabitats may require lower drug doses to induce population decline, whereas sparsely connected structures may necessitate higher drug doses to achieve the same effect.

Spatial drug heterogeneity effect under the same multi-microhabitat structure

For complex systems, researchers often seek a few "coarse-grained" parameters to capture and predict complex behaviors. In our framework, the desired population-level

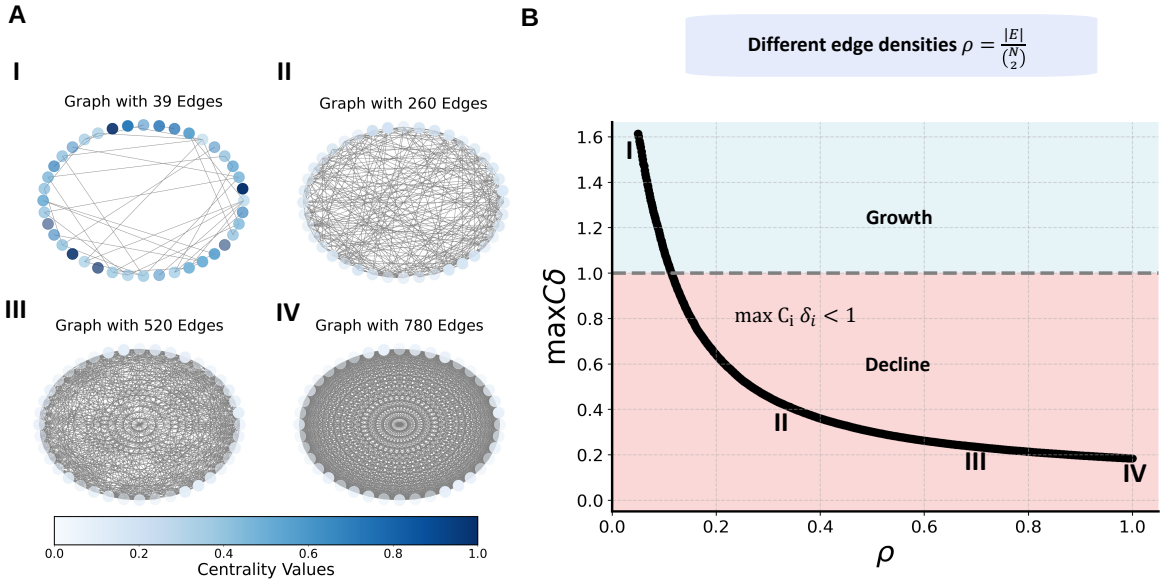

Figure 3. Increasing edge/connection density enhances the tendency for population decline. A. Four example microhabitat structures(microhabitat number $N = 40$) with varying connection densities but the same spatial growth rate distribution. Color gradients represent dynamic-related centrality values C, while different transparencies indicate relative growth values δ. As connectivity increases, the colors gradually fade to white, indicating lower centrality values. **B.** The maximum $C\delta$ value decreases as connection density ρ increases. As the curve crosses the critical threshold $\max C\delta = 1$, population response shifts from growth to decline. Connectivity has a similar effect to migration rate (see SI). The curve represents an average over 1000 stochastic samples of different random networks for each edge density.

response is robust decline, independent of spatial drug heterogeneity. To achieve this, we select the migration rate β and the spatially averaged growth rate $\langle g \rangle$ as key parameters. Our goal is to determine whether a "robust decline" phase exists for a given multi-habitat structure, across different values of β and $\langle g \rangle$, since spatial drug arrangements in human bodies are typically dynamic. Specifically, β and $\langle g \rangle$ are two personalized parameters that depend on the diffusion and drug penetration dynamics of individual patients. Our goal is to determine whether conditions exist that guarantee bacterial or cancer cell clearance across a diverse patient population, while accounting for individual variations in migration and different drug doses.

This problem can be framed as a "constrained optimization problem," as in [44], but finding an exact optimal solution is challenging. Instead, we propose an alternative approach to derive the robust decline phase by leveraging the decoupling of structural and growth information from our criterion. Additionally, we investigate how this phase varies across realistic multi-microhabitat structures and how it depends on the ratio between the maximum growth rate g_0 (which varies with bacterial strain and environmental conditions) and the maximum death rate d_0 (which depends on bacterial type, drug type, and environmental factors).

A sufficient theoretical condition captures robust population decline phase, governed by migration and spatially averaged growth rate

To derive the theoretical condition for robust decline, since we can arbitrarily tune the growth assignment, we require

$$\max C_i \max \delta_i < 1 \tag{3}$$

as shown in Figure 4A. Here the maximum possible relative growth $\delta_{\max}$ is assigned to the microhabitat with the largest dynamic-related centrality $C_{\max}$. By applying an interpolation inequality to $C_{\max}$ and performing a rearrangement (for details, see SI), we obtain the sufficient condition for robust population decline:

$$\beta > \frac{|d_0|}{k_{\min}\left(1 + \frac{1}{\delta_{\max}-1}\right) - \omega_{\max}} \tag{4}$$

This condition becomes exact when the multi-microhabitat structure is a complete graph, where all nonzero Laplacian eigenvalues are equal (see SI). Figure 4B illustrates a phase diagram for a cycle graph with 12 microhabitats, where our sufficient condition provides a lower bound for the numerical boundary of the robust decline phase.

In cancer research, the star graph is of particular interest, as it models metastasis from a primary site to different distant locations [48, 50]. Similarly, in bacterial populations, certain microhabitats may be fully connected [66, 67]. We analyze robust decline phases for both star and complete graphs under varying drug-free growth rates g_0. Our results indicate that decreasing g_0 expands the robust decline phase, as shown in Figure 4C. This observation is reasonable, as lower g_0 requires more microhabitats with positive growth rates to balance the reduced upper growth bound. Notably, our sufficient condition precisely matches the numerical boundary when all microhabitats are fully connected (complete graph, Figure 4C, bottom panel).

Drug-related ratio of drug-free growth and drug-induced death determines minimal phase of robust decline

In our framework, once the nutrient conditions, bacterial type, and drug type are fixed, the values of g_0 and d_0 remain constant. Interestingly, increasing g_0 reduces the phase area of robust decline, thereby narrowing the range of parameters, such as total drug dose, that can be chosen. This suggests that decreasing d_0 may, conversely, expand the robust decline phase. Therefore, we focus on the ratio of drug-free growth g_0 to maximum drug-induced death d_0, which serves as an intrinsic characteristic of the drug-cell interaction.

Notably, when $\frac{|g_0|}{|d_0|}$ exceeds a critical value, the phase area stabilizes instead of shrinking to zero, leading to a minimal robust decline phase. As illustrated in Figure 5A, for a fully connected multi-habitat structure, the phase size remains unchanged for initial reductions in $\frac{|g_0|}{|d_0|}$; however, further decreases cause the phase size to shrink. This phenomenon can be explained by the upper bound of the growth rate: if this bound is too high, even when the spatially averaged growth rate is small, filling all other microhabitats with the maximum death rate is insufficient to counterbalance the highest centrality microhabitat's maximum growth rate. This defines a critical growth-death ratio, as shown in Figure 5B. This critical value depends solely on the microhabitat structure and is independent of dynamic details. For a complete graph, we can derive this critical value exactly. By measuring g_0 and d_0 from experimental data, we can construct a g_0-d_0 plot (Figure 5C), where the critical value appears as a slope dividing

the data into different phases. Importantly, the position of this slope shifts depending on the underlying multi-microhabitat structure, but it still provides valuable health-related dosage guidance when the structure is known. Each colored dot in Figure 5C represents a different nutrient-bacteria pair. While the overall dataset exhibits a linear trend, its nonzero y-intercept indicates the presence of certain nutrient-bacteria pairs with minimal phases. This is a crucial consideration when prescribing drug dosages to patients, as a smaller robust decline phase decreases the likelihood of successfully eliminating bacteria or cancer in the human body. Experimental data are sourced from [60], with additional comparisons to drug tolerance data (see SI).

Discussion

Complex biological systems, such as cancer and bacterial populations, are intertwined with network structures, growth dynamics, and interactions. In this study, we derived a theoretical criterion that guarantees population-level responses for any given multi-microhabitat structure within a spatially heterogeneous drug environment. Our findings reveal that increasing connections between microhabitats promotes population decline, mirroring the effect of an increased migration rate. Moreover, we identified a robust decline phase, wherein the population always declines regardless of spatial drug heterogeneity, by tuning the migration rate and the spatially averaged growth rate. We established a sufficient theoretical condition for this phase, which becomes exact when the microhabitat structure is a complete graph. The growth rates induced by drugs are not arbitrary but are constrained by the drug-free growth rate, which depends on the specific cell type and nutrient conditions, and the maximum death rate, which is determined by the drug and cell type. We found that increasing the growth-to-death ratio reduces the robust decline phase area, and beyond a critical ratio, a minimal robust decline phase persists rather than shrinking to zero. By mapping experimentally or clinically derived growth-death data to these ratios, we can gain a better understanding of clinical and experimental response outcomes.

Across-node properties such as centrality measures play a crucial role in graph theory and network analysis. For instance, subgraph centrality quantifies node importance based on participation in subgraphs [68], with a bias toward smaller subgraphs. Interestingly, our dynamic-related centrality C exhibits an inverse relationship with node degree, contrasting with traditional centrality measures such as Katz or eigenvalue centrality [69, 70]. Recent work on dynamic centrality has aimed to integrate both topological and dynamical properties of nodes to more accurately identify influential spreaders in static and temporal networks [71–73]. These studies emphasize the importance of incorporating temporal aspects into centrality metrics, as static measures fail to capture the evolving nature of real-world networks, crucial for predicting node importance in dynamic systems [72, 74]. Empirical studies demonstrate that these methods outperform conventional metrics across various scenarios, including information and disease spreading [73, 74]. However, previous formulations of dynamic centrality primarily focus on the addition or deletion of nodes within a network, meaning they remain fundamentally structural measures that describe the dynamics of the network itself. In contrast, our dynamic-related centrality focuses on the dynamics occurring on the network. This distinction makes our proposed measure novel, and we term it "dynamic-related centrality" to distinguish it from "dynamic centrality" for the dynamics of the network. We anticipate that this new centrality will expand existing centrality classifications and provide direct insights into dynamic properties without requiring complex simulations. Interestingly, our dynamic-related centrality C also shares a mathematical form with the regularized Laplacian kernel [75], a graph similarity measure based on the Laplacian matrix L. The regularized Laplacian kernel is

defined as: $K = (I + \alpha L)^{-1}$, where I is the identity matrix, L is the Laplacian matrix defined as $L = D - A$ (with D as the degree matrix and A as the adjacency matrix), and $\alpha > 0$ is a regularization parameter controlling the influence of the Laplacian. Setting $\alpha = \frac{\beta}{|d_0|}$ aligns the RLK formulation with our centrality C. However, our dynamic-related centrality differs from the regularized Laplacian kernel in key ways. First, C explicitly incorporates the migration rate β, making it a genuinely dynamic centrality with meaningful biological interpretation rather than just a tunable parameter. Second, while RLK focuses on off-diagonal elements to quantify node similarities, our measure focuses on diagonal elements, aligning with the concept of centrality. Establishing connections between our new dynamic centrality and existing graph properties enhances its interpretability and potential applications.

Understanding population responses to drug treatment, such as antibiotics or chemotherapy, is critical for assessing therapeutic success. Recent studies in both bacterial and cancer systems have identified an interesting phenomenon known as "bistability", where small differences in key parameters—such as drug concentration or growth rate—can lead to drastically different outcomes [76–80]. This concept helps explain variability in clinical outcomes. Here, we propose an alternative explanation for such bi-outcome scenarios: spatial drug heterogeneity and differences in microhabitat connectivity may also contribute to distinct clearance outcomes, independent of bistability. This insight could inform the development of new treatment strategies tailored to spatial drug distribution patterns.

Experimental studies have demonstrated the impact of spatial structure on growth [44, 81], competition, and evolution [82–85]. Our theoretical findings may aid in the interpretation of experimental results and guide the design of future studies. Combining theoretical and experimental approaches can enhance our understanding and contribute to the development of spatially explicit drug dosing strategies.

This study explored population responses across various microhabitat structures and spatial drug heterogeneities, revealing insights beyond previous research that primarily focused on homogeneous structures and drug distributions. However, several extensions remain for future research. First, we considered only non-frequency-dependent drug-induced growth in a single cell type. Although experimental or clinical data on drug-mediated growth interactions remain scarce, some recent studies have begun to address this gap [86, 87]. Future work could incorporate frequency-dependent growth effects and multi-species interactions using evolutionary game theory [88–92] to uncover additional theoretical results and experimental comparisons. Second, we did not account for temporal drug decay or fluctuations in our models. Future work could integrate spatial-temporal drug variations based on patient-specific pharmacokinetics/pharmacodynamics (PK/PD) [25] to inform personalized treatment strategies that ensure bacterial or cancer clearance.

Acknowledgments

This study was supported by NIH R35GM124875 (K. W.).

References

1. K. Wood, "Microbial ecology: complex bacterial communities reduce selection for antibiotic resistance," *Current biology*, vol. 29, no. 21, pp. R1143–R1145, 2019.

2. M. Denk-Lobnig and K. B. Wood, "Antibiotic resistance in bacterial communities," *Current Opinion in Microbiology*, vol. 74, p. 102306, 2023.

3. G. Aguadé-Gorgorió, A. R. Anderson, and R. Solé, "Modeling tumors as complex ecosystems," *Iscience*, vol. 27, no. 9, 2024.

4. E. Hansen, J. Karslake, R. J. Woods, A. F. Read, and K. B. Wood, "Antibiotics can be used to contain drug-resistant bacteria by maintaining sufficiently large sensitive populations," *PLoS biology*, vol. 18, no. 5, p. e3000713, 2020.

5. J. A. Gallaher, P. M. Enriquez-Navas, K. A. Luddy, R. A. Gatenby, and A. R. Anderson, "Spatial heterogeneity and evolutionary dynamics modulate time to recurrence in continuous and adaptive cancer therapies," *Cancer research*, vol. 78, no. 8, pp. 2127–2139, 2018.

6. J. West, F. Adler, J. Gallaher, M. Strobl, R. Brady-Nicholls, J. Brown, M. Roberson-Tessi, E. Kim, R. Noble, Y. Viossat, *et al.*, "A survey of open questions in adaptive therapy: Bridging mathematics and clinical translation," *Elife*, vol. 12, p. e84263, 2023.

7. M. A. Strobl, A. L. Martin, J. West, J. Gallaher, M. Robertson-Tessi, R. Gatenby, R. Wenham, P. K. Maini, M. Damaghi, and A. R. Anderson, "To modulate or to skip: De-escalating parp inhibitor maintenance therapy in ovarian cancer using adaptive therapy," *Cell Systems*, vol. 15, no. 6, pp. 510–525, 2024.

8. K. Gallagher, M. A. Strobl, D. S. Park, F. C. Spoendlin, R. A. Gatenby, P. K. Maini, and A. R. Anderson, "Mathematical model-driven deep learning enables personalized adaptive therapy," *Cancer Research*, vol. 84, no. 11, pp. 1929–1941, 2024.

9. P. P. Chakraborty, L. R. Nemzer, and R. Kassen, "Experimental evidence that metapopulation structure can accelerate adaptive evolution," *BioRxiv*, pp. 2021–07, 2021.

10. A. Wu, K. Loutherback, G. Lambert, L. Estévez-Salmerón, T. D. Tlsty, R. H. Austin, and J. C. Sturm, "Cell motility and drug gradients in the emergence of resistance to chemotherapy," *Proceedings of the National Academy of Sciences*, vol. 110, no. 40, pp. 16103–16108, 2013.

11. Q. Zhang, G. Lambert, D. Liao, H. Kim, K. Robin, C.-k. Tung, N. Pourmand, and R. H. Austin, "Acceleration of emergence of bacterial antibiotic resistance in connected microenvironments," *Science*, vol. 333, no. 6050, pp. 1764–1767, 2011.

12. M. Baym, T. D. Lieberman, E. D. Kelsic, R. Chait, R. Gross, I. Yelin, and R. Kishony, "Spatiotemporal microbial evolution on antibiotic landscapes," *Science*, vol. 353, no. 6304, pp. 1147–1151, 2016.

13. K. Nagy, B. Dukic, O. Hodula, Á. Ábrahám, E. Csákvári, L. Dér, M. T. Wetherington, J. Noorlag, J. E. Keymer, and P. Galajda, "Emergence of resistant escherichia coli mutants in microfluidic on-chip antibiotic gradients," *Frontiers in microbiology*, vol. 13, p. 820738, 2022.

14. G. G. Perron, A. Gonzalez, and A. Buckling, "Source–sink dynamics shape the evolution of antibiotic resistance and its pleiotropic fitness cost," *Proceedings of the Royal Society B: Biological Sciences*, vol. 274, no. 1623, pp. 2351–2356, 2007.

15. R. M. Wheatley, J. D. Caballero, T. E. van der Schalk, F. H. De Winter, L. P. Shaw, N. Kapel, C. Recanatini, L. Timbermont, J. Kluytmans, M. Esser, *et al.*, "Gut to lung translocation and antibiotic mediated selection shape the dynamics of pseudomonas aeruginosa in an icu patient," *Nature communications*, vol. 13, no. 1, p. 6523, 2022.

16. R. Hermsen and T. Hwa, "Sources and sinks: a stochastic model of evolution in heterogeneous environments," *Physical review letters*, vol. 105, no. 24, p. 248104, 2010.

17. R. Hermsen, J. B. Deris, and T. Hwa, "On the rapidity of antibiotic resistance evolution facilitated by a concentration gradient," *Proceedings of the National Academy of Sciences*, vol. 109, no. 27, pp. 10775–10780, 2012.

18. D. Labavić, C. Loverdo, and A.-F. Bitbol, "Hydrodynamic flow and concentration gradients in the gut enhance neutral bacterial diversity," *Proceedings of the National Academy of Sciences*, vol. 119, no. 1, p. e2108671119, 2022.

19. F. Baquero, M.-C. Negri, M.-I. Morosini, and J. Blázquez, "Antibiotic-selective environments," *Clinical infectious diseases*, vol. 27, no. Supplement_1, pp. S5–S11, 1998.

20. T. B. Kepler and A. S. Perelson, "Drug concentration heterogeneity facilitates the evolution of drug resistance," *Proceedings of the National Academy of Sciences*, vol. 95, no. 20, pp. 11514–11519, 1998.

21. P. Greulich, B. Waclaw, and R. J. Allen, "Mutational pathway determines whether drug gradients accelerate evolution of drug-resistant cells," *Physical review letters*, vol. 109, no. 8, p. 088101, 2012.

22. L. Marrec and A.-F. Bitbol, "Adapt or perish: Evolutionary rescue in a gradually deteriorating environment," *Genetics*, vol. 216, no. 2, pp. 573–583, 2020.

23. H. Steel and A. Papachristodoulou, "The effect of spatiotemporal antibiotic inhomogeneities on the evolution of resistance," *Journal of theoretical biology*, vol. 486, p. 110077, 2020.

24. A. I. Klimenko, Y. G. Matushkin, N. A. Kolchanov, and S. A. Lashin, "Spatial heterogeneity promotes antagonistic evolutionary scenarios in microbial community explained by ecological stratification: a simulation study," *Ecological modelling*, vol. 399, pp. 66–76, 2019.

25. H. Xie, Y. Jiao, Q. Fan, M. Hai, J. Yang, Z. Hu, Y. Yang, J. Shuai, G. Chen, R. Liu, *et al.*, "Modeling three-dimensional invasive solid tumor growth in heterogeneous microenvironment under chemotherapy," *PloS one*, vol. 13, no. 10, p. e0206292, 2018.

26. J. Deng, L. Zhou, R. A. Sanford, L. A. Shechtman, Y. Dong, R. E. Alcalde, M. Sivaguru, G. A. Fried, C. J. Werth, and B. W. Fouke, "Adaptive evolution of escherichia coli to ciprofloxacin in controlled stress environments: contrasting patterns of resistance in spatially varying versus uniformly mixed concentration conditions," *Environmental Science & Technology*, vol. 53, no. 14, pp. 7996–8005, 2019.

27. A. M. Leale and R. Kassen, "The emergence, maintenance, and demise of diversity in a spatially variable antibiotic regime," *Evolution Letters*, vol. 2, no. 2, pp. 134–143, 2018.

28. R. C. MacLean and T. Vogwill, "Limits to compensatory adaptation and the persistence of antibiotic resistance in pathogenic bacteria," *Evolution, medicine, and public Health*, vol. 2015, no. 1, pp. 4–12, 2015.

29. S. Xu, *Evolution of Microbial Interactions*. PhD thesis, University of Miami, 2020.

30. B. Zhang, L. Zhai, J. Bintz, S. M. Lenhart, W. Valega-Mackenzie, and J. D. Van Dyken, "The optimal controlling strategy on a dispersing population in a two-patch system: Experimental and theoretical perspectives," *Journal of theoretical biology*, vol. 528, p. 110835, 2021.

31. A. Abbara and A.-F. Bitbol, "Frequent asymmetric migrations suppress natural selection in spatially structured populations," *bioRxiv*, pp. 2023–06, 2023.

32. P. Amarasekare, "Competitive coexistence in spatially structured environments: a synthesis," *Ecology letters*, vol. 6, no. 12, pp. 1109–1122, 2003.

33. Y. Liang, S. McDonnell, and M. Clynes, "Examining the relationship between cancer invasion/metastasis and drug resistance," *Current cancer drug targets*, vol. 2, no. 3, pp. 257–277, 2002.

34. J. Hansen, *Heterogeneity and the Evolution of Drug Resistance*. PhD thesis, University of Michigan, 2023.

35. F. Fu, M. A. Nowak, and S. Bonhoeffer, "Spatial heterogeneity in drug concentrations can facilitate the emergence of resistance to cancer therapy," *PLoS computational biology*, vol. 11, no. 3, p. e1004142, 2015.

36. V. Piskovsky and N. M. Oliveira, "Bacterial motility can govern the dynamics of antibiotic resistance evolution," *Nature Communications*, vol. 14, no. 1, p. 5584, 2023.

37. L. Marrec, I. Lamberti, and A.-F. Bitbol, "Toward a universal model for spatially structured populations," *Physical review letters*, vol. 127, no. 21, p. 218102, 2021.

38. O. M. Ghosh and B. H. Good, "Emergent evolutionary forces in spatial models of luminal growth and their application to the human gut microbiota," *Proceedings of the National Academy of Sciences*, vol. 119, no. 28, p. e2114931119, 2022.

39. M. G. De Jong and K. B. Wood, "Tuning spatial profiles of selection pressure to modulate the evolution of drug resistance," *Physical review letters*, vol. 120, no. 23, p. 238102, 2018.

40. M. De Jong, *Emergence of Antibiotic Resistance in Microbial Populations with Spatial Heterogeneity*. PhD thesis, University of Michigan, 2021.

41. J. T. Lamont, "Patient education: Helicobacter pylori infection and treatment (beyond the basics)," 2022.

42. R. Dent, M. Trudeau, K. I. Pritchard, W. M. Hanna, H. K. Kahn, C. A. Sawka, L. A. Lickley, E. Rawlinson, P. Sun, and S. A. Narod, "Triple-negative breast cancer: clinical features and patterns of recurrence," *Clinical cancer research*, vol. 13, no. 15, pp. 4429–4434, 2007.

43. A. I. Riggio, K. E. Varley, and A. L. Welm, "The lingering mysteries of metastatic recurrence in breast cancer," *British journal of cancer*, vol. 124, no. 1, pp. 13–26, 2021.

44. Z. Hu, Y. Wu, T. Freire, E. Gjini, and K. Wood, "Linking spatial drug heterogeneity to microbial growth dynamics in theory and experiment," *bioRxiv*, pp. 2024–11, 2024.

45. T. F. A. Freire, Z. Hu, K. B. Wood, and E. Gjini, "Modeling spatial evolution of multi-drug resistance under drug environmental gradients," *PLOS Computational Biology*, vol. 20, no. 5, p. e1012098, 2024.

46. L. Chen, N. Blumm, N. Christakis, A. Barabasi, and T. S. Deisboeck, "Cancer metastasis networks and the prediction of progression patterns," *British journal of cancer*, vol. 101, no. 5, pp. 749–758, 2009.

47. L. d. F. Costa, O. N. Oliveira Jr, G. Travieso, F. A. Rodrigues, P. R. Villas Boas, L. Antiqueira, M. P. Viana, and L. E. Correa Rocha, "Analyzing and modeling real-world phenomena with complex networks: a survey of applications," *Advances in Physics*, vol. 60, no. 3, pp. 329–412, 2011.

48. M. Riihimäki, A. Hemminki, M. Fallah, H. Thomsen, K. Sundquist, J. Sundquist, and K. Hemminki, "Metastatic sites and survival in lung cancer," *Lung cancer*, vol. 86, no. 1, pp. 78–84, 2014.

49. M. Riihimäki, H. Thomsen, K. Sundquist, J. Sundquist, and K. Hemminki, "Clinical landscape of cancer metastases," *Cancer medicine*, vol. 7, no. 11, pp. 5534–5542, 2018.

50. X. Jin, Z. Demere, K. Nair, A. Ali, G. B. Ferraro, T. Natoli, A. Deik, L. Petronio, A. A. Tang, C. Zhu, *et al.*, "A metastasis map of human cancer cell lines," *Nature*, vol. 588, no. 7837, pp. 331–336, 2020.

51. N. L. Trevaskis, L. M. Kaminskas, and C. J. Porter, "From sewer to saviour—targeting the lymphatic system to promote drug exposure and activity," *Nature reviews Drug discovery*, vol. 14, no. 11, pp. 781–803, 2015.

52. T. Kodama, D. Matsuki, A. Tada, K. Takeda, and S. Mori, "New concept for the prevention and treatment of metastatic lymph nodes using chemotherapy administered via the lymphatic network," *Scientific reports*, vol. 6, no. 1, p. 32506, 2016.

53. H. Ji, C. Hu, X. Yang, Y. Liu, G. Ji, S. Ge, X. Wang, and M. Wang, "Lymph node metastasis in cancer progression: molecular mechanisms, clinical significance and therapeutic interventions," *Signal Transduction and Targeted Therapy*, vol. 8, no. 1, p. 367, 2023.

54. M. Ziaka and A. Exadaktylos, "Exploring the lung-gut direction of the gut-lung axis in patients with ards," *Critical Care*, vol. 28, no. 1, p. 179, 2024.

55. M. W. Eladham, B. Selvakumar, N. S. Sharif-Askari, F. S. Sharif-Askari, S. M. Ibrahim, and R. Halwani, "Unraveling the gut-lung axis: Exploring complex mechanisms in disease interplay," *Heliyon*, 2024.

56. J. Coates, B. R. Park, D. Le, E. Şimşek, W. Chaudhry, and M. Kim, "Antibiotic-induced population fluctuations and stochastic clearance of bacteria," *Elife*, vol. 7, p. e32976, 2018.

57. N. G. Van Kampen, *Stochastic processes in physics and chemistry*, vol. 1. Elsevier, 1992.

58. A. J. Lee, S. Wang, H. R. Meredith, B. Zhuang, Z. Dai, and L. You, "Robust, linear correlations between growth rates and β-lactam–mediated lysis rates," *Proceedings of the National Academy of Sciences*, vol. 115, no. 16, pp. 4069–4074, 2018.

59. S. Pearl Mizrahi, A. Goyal, and J. Gore, "Community interactions drive the evolution of antibiotic tolerance in bacteria," *Proceedings of the National Academy of Sciences*, vol. 120, no. 3, p. e2209043119, 2023.

60. A. Bren, D. S. Glass, Y. K. Kohanim, A. Mayo, and U. Alon, "Tradeoffs in bacterial physiology determine the efficiency of antibiotic killing," *Proceedings of the National Academy of Sciences*, vol. 120, no. 51, p. e2312651120, 2023.

61. L. Geyrhofer, P. Ruelens, A. D. Farr, D. Pesce, J. A. G. de Visser, and N. Brenner, "Minimal surviving inoculum in collective antibiotic resistance," *Mbio*, vol. 14, no. 2, pp. e02456–22, 2023.

62. S. C. Ferreira, C. Castellano, and R. Pastor-Satorras, "Epidemic thresholds of the susceptible-infected-susceptible model on networks: A comparison of numerical and theoretical results," *Physical Review E—Statistical, Nonlinear, and Soft Matter Physics*, vol. 86, no. 4, p. 041125, 2012.

63. C. Li, R. van de Bovenkamp, and P. Van Mieghem, "Susceptible-infected-susceptible model: A comparison of n-intertwined and heterogeneous mean-field approximations," *Physical Review E—Statistical, Nonlinear, and Soft Matter Physics*, vol. 86, no. 2, p. 026116, 2012.

64. E. Cator and P. Van Mieghem, "Susceptible-infected-susceptible epidemics on the complete graph and the star graph: Exact analysis," *Physical Review E—Statistical, Nonlinear, and Soft Matter Physics*, vol. 87, no. 1, p. 012811, 2013.

65. H. Chen, G. Li, H. Zhang, and Z. Hou, "Optimal allocation of resources for suppressing epidemic spreading on networks," *Physical Review E*, vol. 96, no. 1, p. 012321, 2017.

66. M. T. Pearce, A. Agarwala, and D. S. Fisher, "Stabilization of extensive fine-scale diversity by ecologically driven spatiotemporal chaos," *Proceedings of the National Academy of Sciences*, vol. 117, no. 25, pp. 14572–14583, 2020.

67. J. Hu, *Emergent behaviors in complex microbial ecosystems*. PhD thesis, Massachusetts Institute of Technology, 2024.

68. E. Estrada and J. A. Rodriguez-Velazquez, "Subgraph centrality in complex networks," *Physical Review E—Statistical, Nonlinear, and Soft Matter Physics*, vol. 71, no. 5, p. 056103, 2005.

69. L. Katz, "A new status index derived from sociometric analysis," *Psychometrika*, vol. 18, no. 1, pp. 39–43, 1953.

70. M. E. Newman, "The mathematics of networks," *The new palgrave encyclopedia of economics*, vol. 2, no. 2008, pp. 1–12, 2008.

71. R. Poulin, M.-C. Boily, and B. R. Mâsse, "Dynamical systems to define centrality in social networks," *Social networks*, vol. 22, no. 3, pp. 187–220, 2000.

72. P. Grindrod and D. J. Higham, "A dynamical systems view of network centrality," *Proceedings of the Royal Society A: Mathematical, Physical and Engineering Sciences*, vol. 470, no. 2165, p. 20130835, 2014.

73. J.-G. Liu, J.-H. Lin, Q. Guo, and T. Zhou, "Locating influential nodes via dynamics-sensitive centrality," *Scientific reports*, vol. 6, no. 1, p. 21380, 2016.

74. D.-W. Huang and Z.-G. Yu, "Dynamic-sensitive centrality of nodes in temporal networks," *Scientific reports*, vol. 7, no. 1, p. 41454, 2017.

75. A. J. Smola and R. Kondor, "Kernels and regularization on graphs," in *Learning Theory and Kernel Machines: 16th Annual Conference on Learning Theory and 7th Kernel Workshop, COLT/Kernel 2003, Washington, DC, USA, August 24-27, 2003. Proceedings*, pp. 144–158, Springer, 2003.

76. L. Dai, D. Vorselen, K. S. Korolev, and J. Gore, "Generic indicators for loss of resilience before a tipping point leading to population collapse," *Science*, vol. 336, no. 6085, pp. 1175–1177, 2012.

77. J. Karslake, J. Maltas, P. Brumm, and K. B. Wood, "Population density modulates drug inhibition and gives rise to potential bistability of treatment outcomes for bacterial infections," *PLoS computational biology*, vol. 12, no. 10, p. e1005098, 2016.

78. J. B. Deris, M. Kim, Z. Zhang, H. Okano, R. Hermsen, A. Groisman, and T. Hwa, "The innate growth bistability and fitness landscapes of antibiotic-resistant bacteria," *Science*, vol. 342, no. 6162, p. 1237435, 2013.

79. N. Frenkel, R. Saar Dover, E. Titon, Y. Shai, and V. Rom-Kedar, "Bistable bacterial growth dynamics in the presence of antimicrobial agents," *Antibiotics*, vol. 10, no. 1, p. 87, 2021.

80. E. S. Wright and K. H. Vetsigian, "Inhibitory interactions promote frequent bistability among competing bacteria," *Nature communications*, vol. 7, no. 1, p. 11274, 2016.

81. A. Limdi, A. Pérez-Escudero, A. Li, and J. Gore, "Asymmetric migration decreases stability but increases resilience in a heterogeneous metapopulation," *Nature Communications*, vol. 9, no. 1, p. 2969, 2018.

82. A. Mishra, P. P. Chakraborty, and S. Dey, "Dispersal evolution diminishes the negative density dependence in dispersal," *Evolution*, vol. 74, no. 9, pp. 2149–2157, 2020.

83. P. P. Chakraborty, L. R. Nemzer, and R. Kassen, "Experimental evidence that network topology can accelerate the spread of beneficial mutations," *Evolution Letters*, vol. 7, no. 6, pp. 447–456, 2023.

84. P. Chakraborty and R. Kassen, "Rapid adaptation and increased genetic parallelism in experimental metapopulations of pseudomonas aeruginosa," *bioRxiv*, pp. 2024–10, 2024.

85. P. P. Chakraborty, *The Impact of Spatial Network Topologies on the Adaptive Evolution of Pseudomonas aeruginosa Metapopulations*. PhD thesis, Université d'Ottawa— University of Ottawa, 2024.

86. N. Farrokhian, J. Maltas, M. Dinh, A. Durmaz, P. Ellsworth, M. Hitomi, E. McClure, A. Marusyk, A. Kaznatcheev, and J. G. Scott, "Measuring competitive exclusion in non–small cell lung cancer," *Science Advances*, vol. 8, no. 26, p. eabm7212, 2022.

87. J. Maltas, D. S. Tadele, A. Durmaz, C. D. McFarland, M. Hinczewski, and J. G. Scott, "Frequency-dependent ecological interactions increase the prevalence, and shape the distribution, of preexisting drug resistance," *PRX Life*, vol. 2, no. 2, p. 023010, 2024.

88. P. Newton and Y. Ma, "Maximizing cooperation in the prisoner's dilemma evolutionary game via optimal control," *Physical Review E*, vol. 103, no. 1, p. 012304, 2021.

89. R. Dua, Y. Ma, and P. K. Newton, "Are adaptive chemotherapy schedules robust? a three-strategy stochastic evolutionary game theory model," *Cancers*, vol. 13, no. 12, p. 2880, 2021.

90. K. Stuckey, R. Dua, Y. Ma, J. Parker, and P. Newton, "Optimal dynamic incentive scheduling for hawk-dove evolutionary games," *Physical Review E*, vol. 105, no. 1, p. 014412, 2022.

91. B. Wölfl, H. Te Rietmole, M. Salvioli, A. Kaznatcheev, F. Thuijsman, J. S. Brown, B. Burgering, and K. Staňková, "The contribution of evolutionary game theory to understanding and treating cancer," *Dynamic Games and Applications*, vol. 12, no. 2, pp. 313–342, 2022.

92. J. Park and P. Newton, "Stochastic competitive release and adaptive chemotherapy," *Physical Review E*, vol. 108, no. 3, p. 034407, 2023.

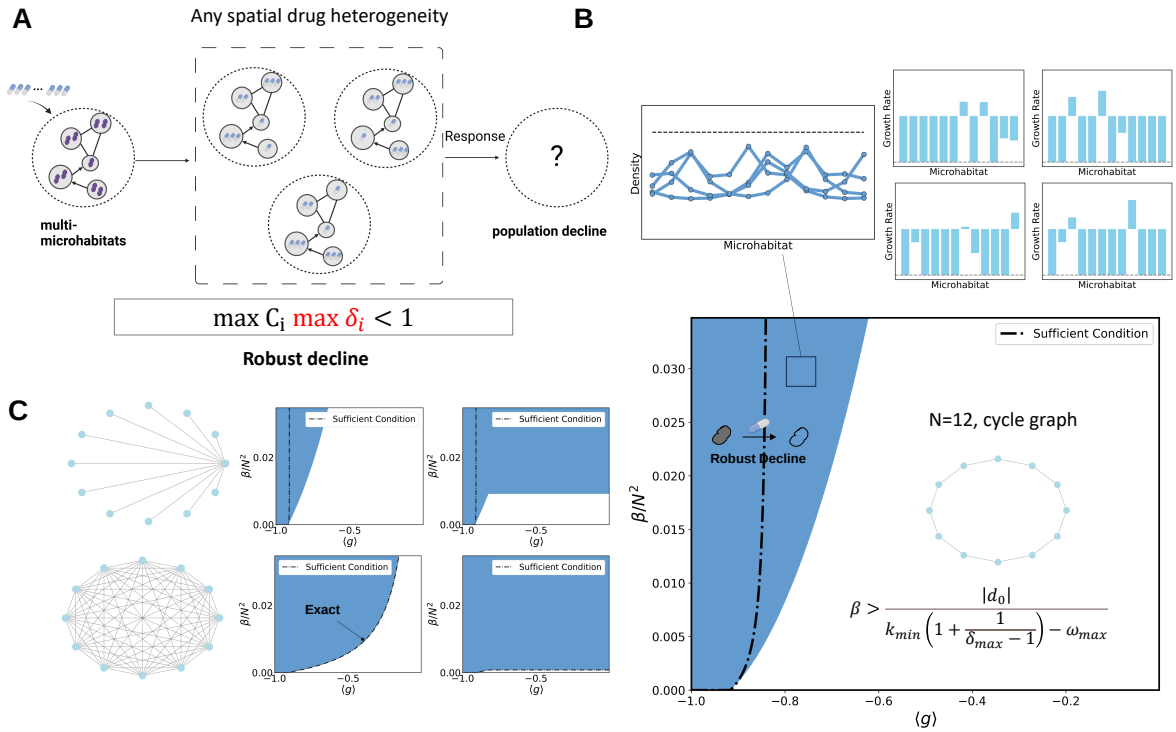

Figure 4. A sufficient theoretical condition for robust population decline, independent of spatial drug heterogeneity. A. Illustration of robust population decline. Regardless of spatial variation, as long as the spatially averaged growth rate $\langle g \rangle$ remains fixed, the population response is always a decline, effectively eliminating the mixed effects of different spatial drug heterogeneities. **B.** Example phase diagram showing the relationship between migration rate β and spatially averaged growth rate $\langle g \rangle$ on a cycle graph as the microhabitat structure. The bottom-right corner highlights the sufficient condition, which depends on migration rate β, maximum death rate d_0, minimum degree $k_{\min}$, maximum Laplacian eigenvalue $\omega_{\max}$, and maximum relative growth $\delta_{\max}$. Above the phase diagram, four different final population densities after a finite time period are displayed, with the dashed line representing the initial uniform population density. Adjacent to the phase diagram, four distinct growth rate distributions are shown. **C.** Phase diagrams for other common microhabitat structures: star and complete graphs, evaluated at different drug-free maximum growth rates g_0 ($g_0 = 22, 1.1$ for the left and right columns, respectively). Decreasing the maximum growth rate expands the robust decline phase. When the structure is a complete graph, the sufficient condition becomes exact, aligning perfectly with the numerical boundary line.

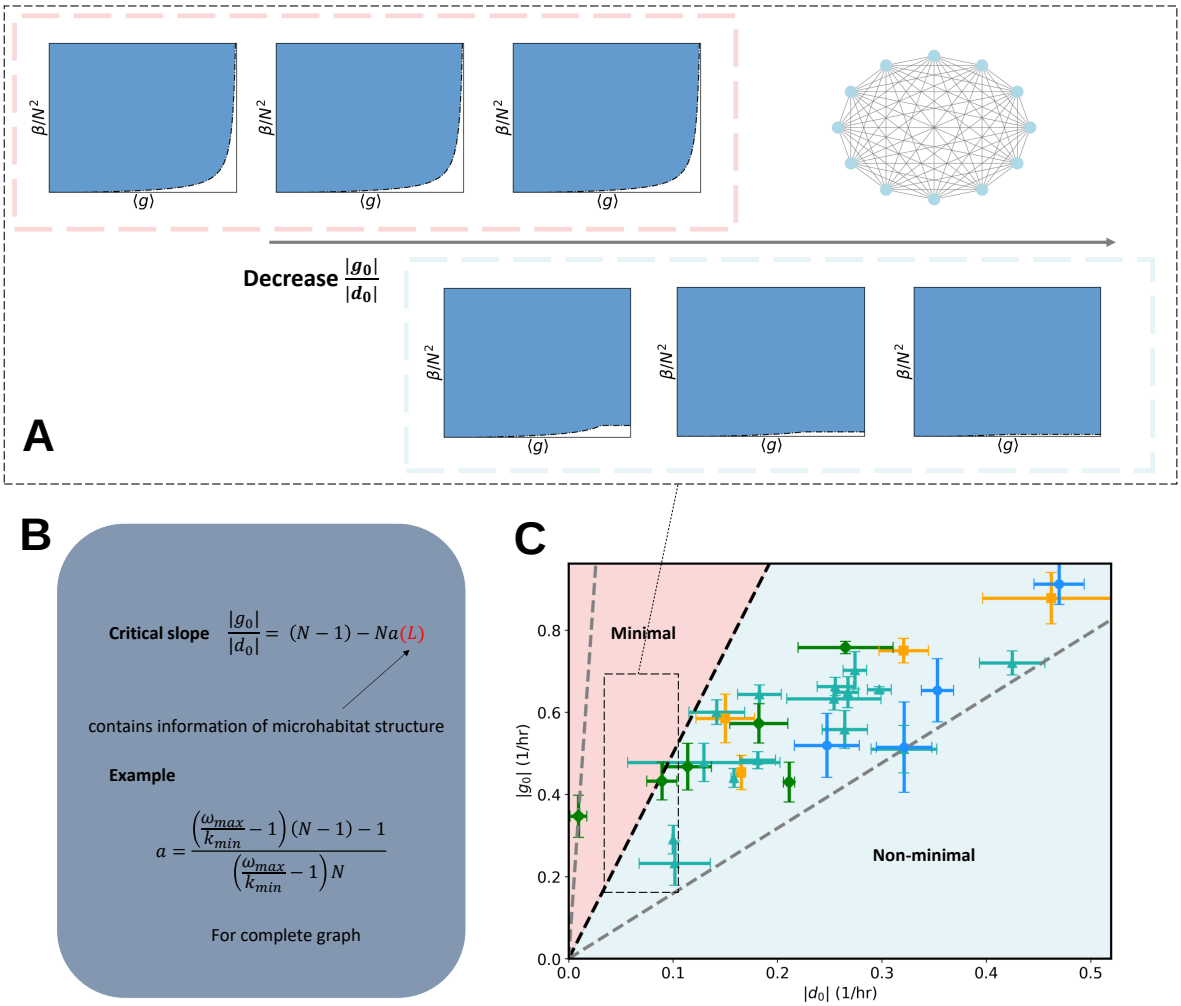

Figure 5. A minimal robust decline phase emerges when the maximum growth-death ratio exceeds a critical value. A. Decreasing the ratio $\frac{|g_0|}{|d_0|}$ expands the robust decline phase. The phase diagrams within the light red rectangle exhibit an invariant minimal phase. **B.** The critical slope of the maximum growth-death ratio is identified, depending solely on microhabitat structure, specifically the structural parameter $a(L)$ and the number of microhabitats N. For a complete graph, the theoretical expression for $a(L)$ can be derived rigorously. **C.** A plot illustrating the minimal robust decline phase and the non-minimal phase, separated by the critical slope. Experimental data with error bars are taken from Bren et al. [60]. Different colors represent distinct environmental conditions paired with various bacterial strains. Some bacteria-environment pairs exhibit a minimal robust decline phase. Note that the critical boundary line depends on the actual microhabitat structure of patients; the one shown here is only an example for illustration.